LETTER

doi:10.1038/nature12148

Synthetic analog computation in living cells

Ramiz Daniel[1,2,3], Jacob R. Rubens[2,3,4], Rahul Sarpeshkar[1,3,4,5,6,7]* & Timothy K. Lu[2,3,4,5,6,8]*

A central goal of synthetic biology is to achieve multi-signal integration and processing in living cells for diagnostic, therapeutic and biotechnology applications[1]. Digital logic has been used to build small-scale circuits, but other frameworks may be needed for efficient computation in the resource-limited environments of cells[2,3]. Here we demonstrate that synthetic analog gene circuits can be engineered to execute sophisticated computational functions in living cells using just three transcription factors. Such synthetic analog gene circuits exploit feedback to implement logarithmically linear sensing, addition, ratiometric and power-law computations. The circuits exhibit Weber's law behaviour as in natural biological systems[4], operate over a wide dynamic range of up to four orders of magnitude and can be designed to have tunable transfer functions. Our circuits can be composed to implement higher-order functions that are well described by both intricate biochemical models and simple mathematical functions. By exploiting analog building-block functions that are already naturally present in cells[3,5], this approach efficiently implements arithmetic operations and complex functions in the logarithmic domain. Such circuits may lead to new applications for synthetic biology and biotechnology that require complex computations with limited parts, need wide-dynamic-range biosensing or would benefit from the fine control of gene expression.

In natural biological systems, digital behaviour is appropriate in settings where decision making is necessary, such as in developmental circuits[6]. The digital approach is an abstraction of graded analog functions, where values above a threshold are classified as '1' and values below this threshold are classified as '0' (Fig. 1a). Digital computation using synthetic gene circuits has included switches, counters, logic gates, classifiers and edge detectors (see references 28–40 in Supplementary Information). However, given that there is often unwanted crosstalk amongst synthetic devices[7] and cellular resource limitations[2,3], it may be challenging to scale digital logic functions to the level needed for complex computations in living cells. Analog functions can be found in natural biological systems, where they enable graded responses to environmental signals[1,8]. For example, neurons can implement both digital and analog computation[9]. Furthermore, electronic circuits that perform analog computation on logarithmically transformed signals have been used in commercially valuable electronic chips for several decades. The thermodynamic Boltzmann exponential equations that describe electron flow in electronic transistors are strikingly mathematically similar to the thermodynamic Boltzmann exponential equations that describe molecular flux in chemical reactions[5]. Their similarities suggest that log-domain analog computation in electronics may be mapped to log-domain analog computation in chemistry, and vice versa[5]. Because analog computation exploits powerful biochemical mathematical basis functions[3,10] that are naturally present over the entire continuous range of input operation (Fig. 1a), they are an advantageous alternative to digital logic when resources of device count, space, time or energy are constrained[2,3].

We first created an analog synthetic gene circuit motif that performs positive, wide-dynamic-range logarithmic transduction of inducer concentration inputs to fluorescent protein outputs (Fig. 1b). The resulting transfer functions have a broad region of linearity on a semi-log plot (log-linear). Logarithmic functions can enable intensity-independent responses and can compress a large input dynamic range into a smaller, manageable output dynamic range. A logarithmic function naturally implements Weber's law behaviour, which states that the ratio between the perceptual change in a signal divided by its background level is a constant, resulting in the detection of fold changes rather than absolute levels[4]. Weber's law is approximately true within molecular signalling networks and in describing human perception of sound intensity, light intensity and weight[4].

Our wide-dynamic-range, positive-logarithm circuit consists of a positive-feedback component located on a low-copy-number plasmid (LCP) and a 'shunt' component located on a high-copy-number plasmid (HCP). The LCP comprises promoters which generate transcription factors that bind to the promoters, thus increasing the generation of transcription factors by means of a positive-feedback loop and alleviating saturation of the interaction between inducers and transcription factors. The HCP comprises promoters that bind and shunt away the generated transcription factors, effectively redirecting some of them away from the LCP and reducing saturation of the interaction between transcription factors and DNA. The HCP shunt also affects the effective strength of the LCP positive-feedback loop. The HCP generates a reporter or protein output that is different from the transcription factor output (Fig. 1b). We initially applied this 'positive-feedback/shunt' (PFS) circuit motif to the AraC transcriptional activator, which is induced by arabinose and activates the P_{BAD} promoter (Fig. 1b and Supplementary Fig. 6).

The AraC-based PFS circuit had an input–output transfer function that was well fitted by a simple mathematical function of the form $\ln(1 + x)$, which is a first-order approximation of the Hill function for small values of x, where x is a scaled version of the input concentration (Fig. 1d and Supplementary Information, section 4). Furthermore, this circuit had a wide input dynamic range of more than three orders of magnitude, where the dynamic range is taken to be the span of inputs over which the output is well fitted by $\ln(x)$ (Fig. 1d and Supplementary Fig. 18). The simple logarithmic mathematical functions that describe our wide-dynamic-range circuits are useful for designing higher-order functions. The wide-dynamic-range behaviour of our circuit was especially striking when compared with the narrow dynamic range of the open-loop control, which has a shunt motif but no positive-feedback motif. This 'open-loop/shunt' motif is shown in Fig. 1c, d and in Supplementary Fig. 16. When the shunt plasmid in the PFS motif contains a P_{lux} promoter rather than a P_{BAD} promoter, wide-dynamic-range logarithmic operation for the AraC-based circuit is also absent (Supplementary Fig. 17). These controls indicate the importance of graded positive feedback, implemented here with the PFS motif, in achieving wide-dynamic-range operation.

[1]Analog Circuits and Biological Systems Group, Research Lab of Electronics, Massachusetts Institute of Technology, Cambridge, Massachusetts 02139, USA. [2]Synthetic Biology Group, Research Lab of Electronics, Massachusetts Institute of Technology, Cambridge, Massachusetts 02139, USA. [3]Synthetic Biology Center, Massachusetts Institute of Technology, Cambridge, Massachusetts 02139, USA. [4]MIT Microbiology Program, Massachusetts Institute of Technology, Cambridge, Massachusetts 02139, USA. [5]Department of Electrical Engineering & Computer Science, Massachusetts Institute of Technology, Cambridge, Massachusetts 02139, USA. [6]MIT Computational and Systems Biology Program, Massachusetts Institute of Technology, Cambridge, Massachusetts 02139, USA. [7]MIT Biophysics Program, Massachusetts Institute of Technology, Cambridge, Massachusetts 02139, USA. [8]Department of Biological Engineering, Massachusetts Institute of Technology, Cambridge, Massachusetts 02139, USA.

*These authors contributed equally to this work.

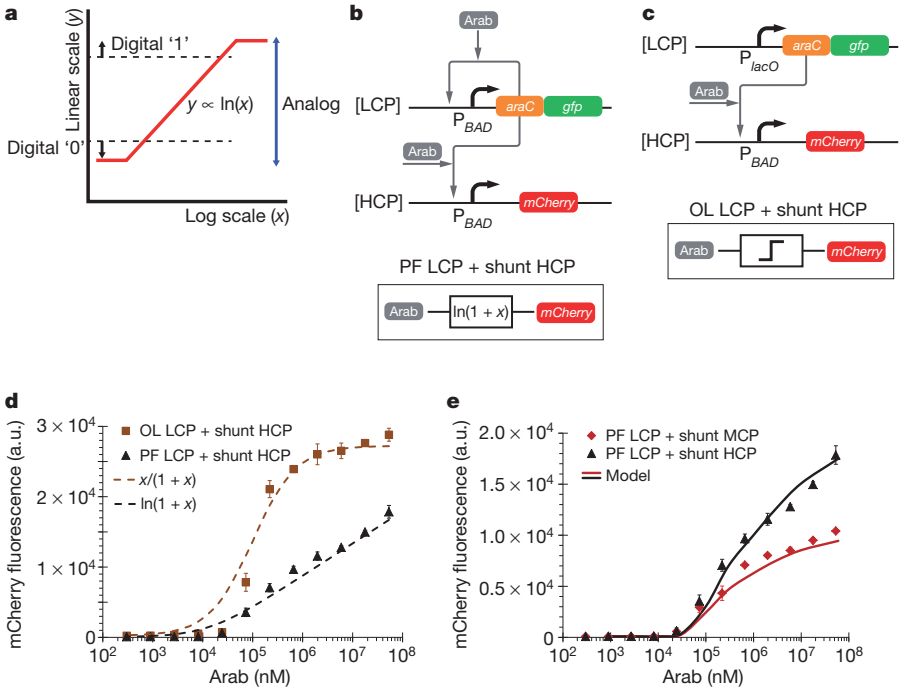

Figure 1 | Positive-feedback linearization of gene circuits for wide-dynamic-range analog computation. **a**, Synthetic analog gene circuits use the inherent continuous behaviour of biochemical reactions to perform computations and implement mathematical functions over a wide dynamic range, whereas digital circuits abstract this behaviour into discrete '0's and '1's. **b**, The AraC-based, wide-dynamic-range, positive-logarithm circuit logarithmically transforms input inducer concentrations into output protein levels. This topology involves a transcriptional positive-feedback (PF) loop on an LCP, which alleviates saturated binding of inducer to transcription factor, along with a shunt HCP containing transcription-factor-binding sites, which alleviates saturation of DNA-binding sites. Arab, arabinose. **c**, The open-loop (OL) control consists of AraC–GFP expression from a P_{lacO} promoter with no positive feedback. **d**, Arabinose-to-mCherry transfer function. The positive-feedback LCP with a shunt HCP (black triangles) implements a wide-dynamic-range, positive-slope logarithm circuit with an input dynamic range of more than three orders of magnitude. It is well fitted by a mathematical function of the form $\ln(1 + x)$, where x is a scaled version of the input inducer concentration. In contrast, the open-loop LCP with a shunt HCP (orange squares) has a narrow dynamic range and is well fitted by a Hill function. a.u., arbitrary units. **e**, Comparing the positive-feedback LCP with a shunt MCP (red diamonds) and the positive-feedback LCP with a shunt HCP (black triangles; data from **d**) demonstrates the importance of the shunt plasmid in making possible the wide-dynamic-range operation. Solid lines indicate modelling results of the detailed biochemical model (Supplementary Information). The errors (s.e.m.) shown in the figures are derived from three flow cytometry experiments, each of which involved $n = 50{,}000$ events.

To gain deeper insights into the mechanisms that may give rise to logarithmically linear transfer functions, we built detailed biochemical models that capture the effects of inducer/transcription-factor binding, transcription-factor/DNA binding, the PFS circuit topology and protein degradation (Fig. 1e and Supplementary Information, section 2). Using a consistent set of model parameters that differ only on the basis of the various circuit topologies (for example in plasmid copy number), our biochemical models accurately capture the behaviour of our multiple circuits (Figs 1 and 2 and Supplementary Fig. 31). A minimal biochemical model, which incorporates only the basic effects of graded positive feedback, also shows linearization (Supplementary Fig. 30). Indeed, our scheme for widening the log-linear dynamic range of operation by means of graded positive feedback is conceptually general and applies to both genetic and electronic circuits: expansive hyperbolic-sine-based linearization of compressive hyperbolic-tangent-based functions in log-domain electronic circuits[11] is analogous to the use of expansive positive-feedback linearization of compressive biochemical binding functions in log-domain genetic circuits.

We generalized these findings to the quorum-sensing transcriptional activator LuxR, which is induced by acyl homoserine lactone (AHL) and activates the promoter P_{lux} (Fig. 2a). As fluorescent outputs of this circuit, we fused green fluorescent protein (GFP) to the carboxy terminus of LuxR and used an HCP P_{lux}-mCherry shunt. The LuxR PFS circuit also had an input dynamic range of more than three orders of magnitude (Fig. 2b) and performed robustly over multiple time points (Supplementary Fig. 26). This input dynamic range was significantly greater than that achieved with LuxR–GFP positive feedback alone or with LuxR–GFP positive feedback with a medium-copy-number plasmid (MCP) shunt (Fig. 2b). The output of the shunt plasmid (mCherry) had similar properties and thus can also be used for computation (Fig. 2c). As in the AraC-based circuits (Fig. 1), both detailed biochemical models (Fig. 2b, c), where the only varying parameter was the plasmid copy number, and the simple $\ln(1 + x)$ mathematical function (Fig. 2b, c, insets) captured the behaviour of the LuxR-based circuits.

The behaviour of the PFS circuit motif can be dynamically tuned by changing the relative copy numbers of the positive-feedback and shunt plasmids. We demonstrated such tuning by combining an HCP shunt with a variable-copy-number plasmid (VCP), based on a pBAC/oriV vector[12], carrying the positive-feedback component (Fig. 2d). When the VCP was induced to a high-copy-number state, the circuit had a narrow dynamic range of about two orders of magnitude and was poorly fitted by a $\ln(1 + x)$ function but could be fitted by a 'digital-like' Hill function (Fig. 2e). When the VCP was in a low-copy-number state, the circuit behaved in an analog fashion, followed a $\ln(1 + x)$ mathematical relationship and had a broad dynamic range of nearly four orders of magnitude. Such tuning demonstrates the importance of the relative copy numbers of the positive-feedback and shunt plasmids in enabling wide-dynamic-range logarithmic operation. It also provides a mechanism for actively changing circuit behaviour between analog and digital modes and shows that the PFS circuit motif can be reliably used in different *Escherichia coli* strain backgrounds.

Our analog computation modules can be composed into more complex circuits for higher-order functions, as shown in Supplementary Information, section 10, and Supplementary Fig. 31. There we show how to compose a wide-dynamic-range PFS logarithm motif with a LacI repressor module to create a wide-dynamic-range negative

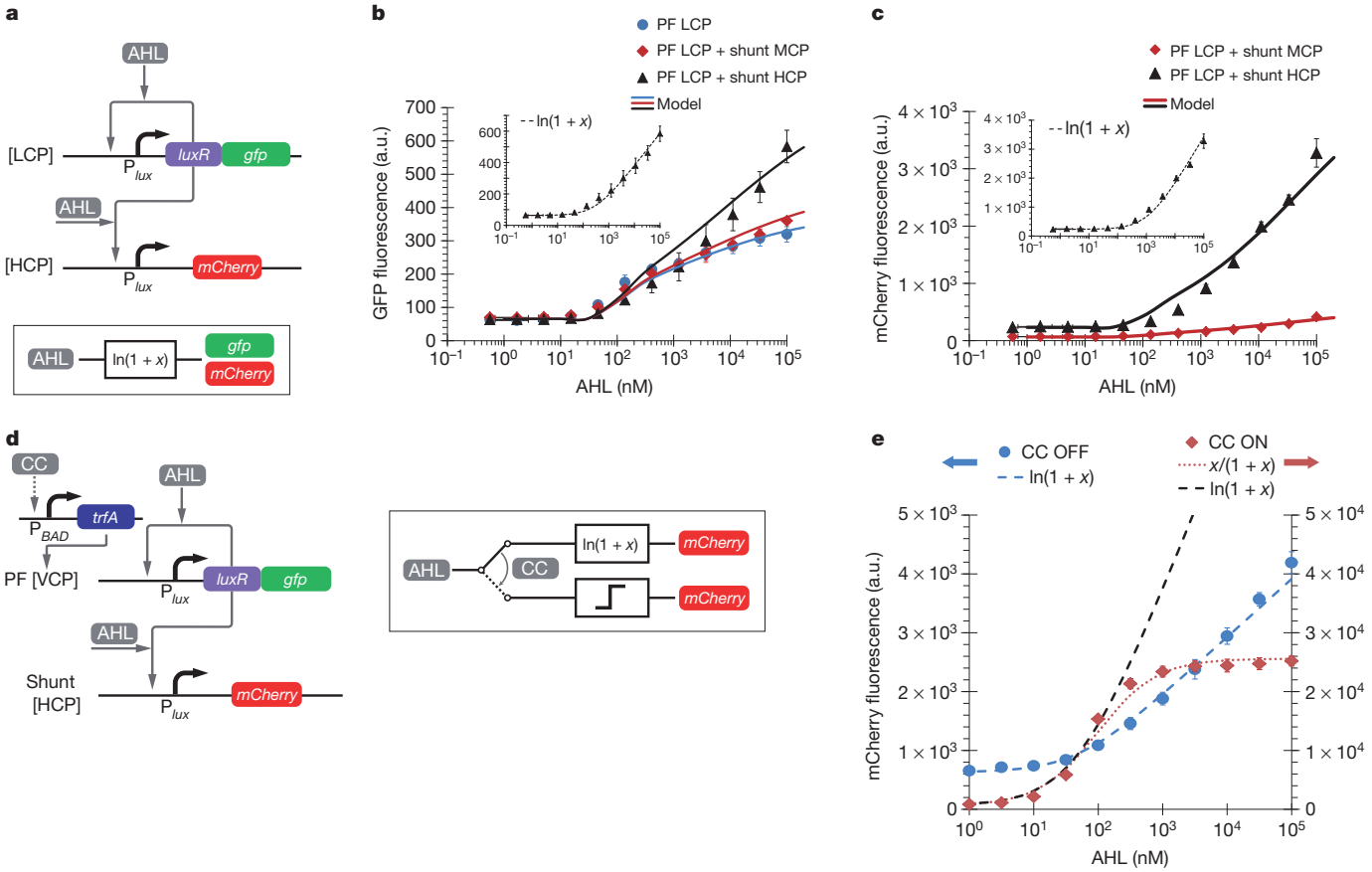

Figure 2 | Analog behaviour versus digital. **a**, The LuxR-based, wide-dynamic-range, positive-logarithm circuit. **b**, The AHL-to-GFP transfer function for a positive-feedback LCP (blue circles), a positive-feedback LCP with a shunt MCP (red diamonds) and a positive-feedback LCP with a shunt HCP (black triangles). The positive-feedback LCP with a shunt HCP implements a wide-dynamic-range, positive-slope logarithm circuit. Solid lines indicate modelling results of the detailed biochemical model; the inset shows the fit of a mathematical function of the form $\ln(1 + x)$. **c**, The AHL-to-mCherry transfer function for a positive-feedback LCP with a shunt MCP (red diamonds) and a positive-feedback LCP with a shunt HCP (black triangles). The positive-feedback LCP with a shunt HCP implements a wide-dynamic-range, positive-slope logarithm circuit. Solid lines indicate modelling results of the detailed biochemical model; the inset shows the fit of a mathematical function of the form $\ln(1 + x)$. **d**, Placing the positive-feedback loop on a VCP allows the dynamic adjustment of AHL-to-mCherry transfer functions between analog and digital behaviours using a CopyControl (CC) induction solution. The VCP is normally maintained at low copy numbers and can be induced to higher copy numbers through CopyControl-mediated expression of replication protein TrfA from a promoter integrated into the genome of EPI300 cells[12]. **e**, At high copy numbers (CC ON, red diamonds), the circuit behaves in a digital-like fashion. The dotted red line is a Hill function fit to the digital-like curve. The dashed black line reveals that the digital-like curve is not well fitted by a $\ln(1 + x)$ function. At low copy numbers (CC OFF, blue circles), the circuit behaves in an analog fashion with a wide dynamic range. The dashed blue line indicates that the PFS positive logarithm is well fitted by a $\ln(1 + x)$ function. The errors (s.e.m.) in the figures are derived from three flow cytometry experiments, each involving $n = 50{,}000$ events.

logarithm motif of the form $-\ln(1 + x)$. The latter motif functions over four orders of magnitude and is well predicted by detailed biochemical models and by compositions of empirical fits.

As an application of synthetic analog genetic circuits, we created an adder circuit that sums its protein inputs, which are logarithmically transformed representations of inducer molecules (Fig. 3a). Such summation is achieved by combining two parallel, wide-dynamic-range, positive-logarithm circuits that accept different input molecules (for example AHL and arabinose) but produce a common output molecule (Fig. 3a). The adder exhibited log-linear behaviour over a range of two orders of magnitude (Fig. 3b and Supplementary Fig. 21). Because log-linear addition of two inputs effectively results in the logarithm of their product, an analog product is equivalent to a 'soft AND' operation, that is, to a graded multiplication rather than to a one-bit digital multiplication. Thus, the data of Fig. 3b have similarities to that obtained from digital AND circuits, except that the overall function is more graded in nature.

We also developed a PFS circuit that calculates the log-transformed ratio of two different input inducers (Fig. 3c). Ratiometric calculations are useful in biological systems, because they enable the normalization of measurements, comparisons between variables and decisions based on competing inputs. Our ratiometer circuit was built by combining a wide-dynamic-range, negative-logarithm circuit and a wide-dynamic-range, positive-logarithm circuit that accept different input molecules but produce a common output molecule (Fig. 3d). This circuit essentially calculates the difference between the log-transformed outputs of the two inputs (subtraction in the log domain). By tuning the ribosome-binding sequences of the negative- and positive-logarithm circuits such that the magnitudes of their slopes are similar, the resulting mathematical function is the log-transformed ratio of the two inputs and functions over four orders of magnitude of this ratio. Our wide-dynamic-range ratiometer enables the concept of pH, which measures the logarithmic concentration ratio of H^+ with respect to an absolute value, to be generalized to the concept of 'pRATIO', which may be useful for measuring the logarithmic concentration ratio of one input with respect to another input.

In addition to logarithmically linear addition and ratiometric calculations, synthetic analog circuits in living cells can implement power laws. To implement such laws, we introduced an inducer/transcription-factor binding function into a strong negative-feedback loop that includes two stages of amplification (Fig. 3e). In the first stage, araC-GFP produced from PlacO on a LCP activates lacI-mCherry produced

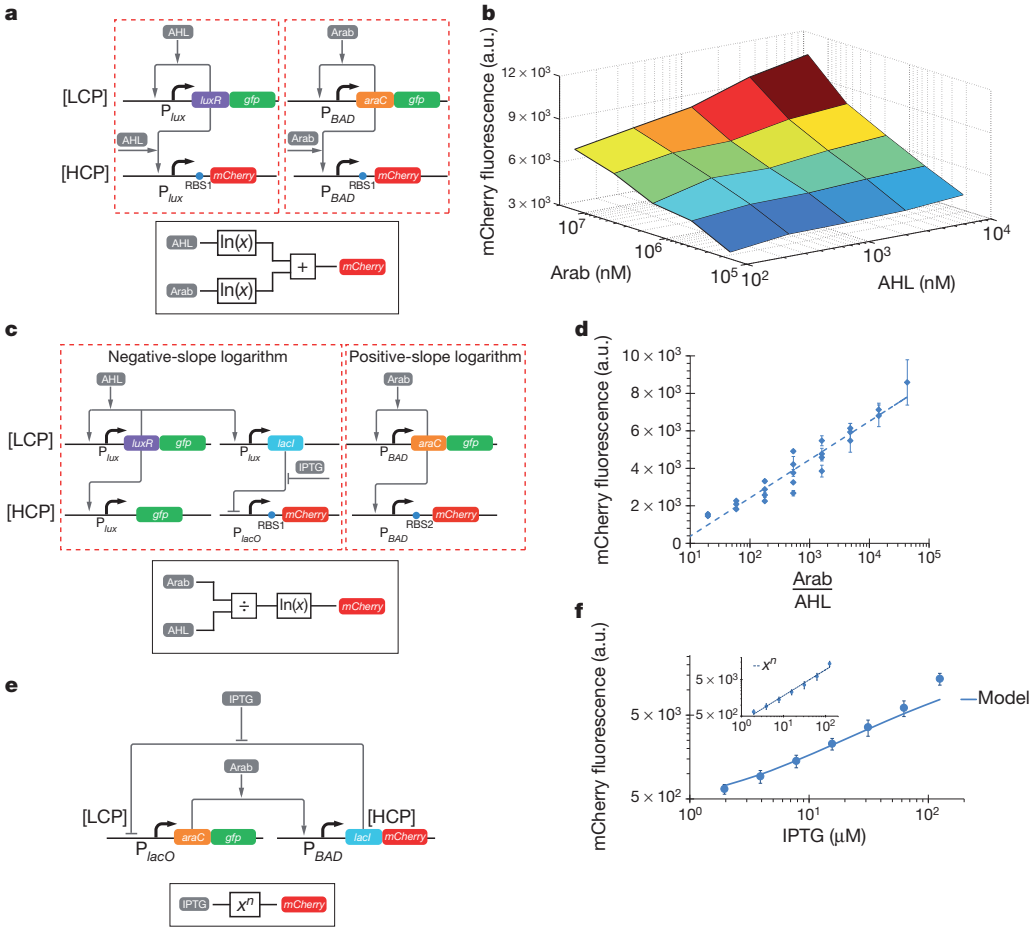

Figure 3 | Log-domain analog computation. Complex analog computation can be implemented by composing synthetic gene circuits. **a**, An adder is built by engineering two wide-dynamic-range, positive-slope logarithm circuits (modules outlined in red) to produce a common output, which is summed to yield the overall output. **b**, The adder circuit sums the logarithms of two inputs, AHL and arabinose, over about two orders of magnitude, to produce an output, mCherry. **c**, A division circuit, or ratiometer, is implemented when the slopes of the wide-dynamic-range, positive- and negative-logarithms (modules outlined in red) are closely matched by tuning their output ribosome-binding sites (RBSs). IPTG, isopropyl-β-D-1-thiogalactopyranoside. **d**, The ratiometer performs a logarithmic transformation on the ratio of two inputs, arabinose and AHL, over more than three orders of magnitude. IPTG was held constant at 1.5 mM. The dotted blue line indicates a log-linear fit. **e**, A negative-feedback loop with tunable feedback strength implements power-law functions. This circuit motif uses LacI–mCherry produced on an HCP to suppress the production of AraC–GFP on an LCP. When induced by arabinose, AraC–GFP enhances the production of LacI–mCherry. **f**, Power-law behaviour can be observed in the IPTG-to-mCherry transfer function, with arabinose constant at 4.6 mM. The solid line indicates modelling results of the detailed biochemical model; the inset shows the fit to a power law of the form $x^{0.7}$. The errors (s.e.m.) shown in the figures are derived from three flow cytometry experiments, each of which involved $n = 50{,}000$ events.

from PBAD on a HCP. In the second stage, LacI-mCherry represses araC-GFP production at PlacO, completing the negative-feedback loop. The power-law nature of our circuit arises from the interactions of saturated-repressor polynomial functions and a linear activator polynomial function in a feedback loop (Supplementary Information, section 2). The power-law behaviour of our circuit extended over two orders of magnitude, was accurately predicted by our detailed biochemical models and was well matched by a simple power law, x^n (Fig. 3f).

We have shown that powerful wide-dynamic-range analog computations can be performed with just a few biological parts in living cells. Four-input-bit, two-output-bit square roots can be calculated *in vitro* using 130 DNA strands within a DNA-based computation framework[13]. In comparison, our *in vivo*, analog power-law circuit exploits binding functions that are already present in the biochemistry and therefore requires only two transcription factors. Even one-bit full adders and subtractors in digital computation require several logic gates and, thus, numerous synthetic parts (refs 34, 35 and 37 Supplementary Information). Our wide-dynamic-range analog adders and ratiometers are inherently implemented by circuits that add flux to or subtract flux from a common output molecule, and can be constructed with no more than three transcription factors (Fig. 3).

In Supplementary Information, section 11, we outline potential applications of our efficient circuit motifs in biotechnology and medicine for fine control of gene expression or wide-dynamic-range sensing. Our wide-dynamic-range analog computation circuits can be further integrated with dynamical systems such as oscillators[14–16], negative-feedback linearizing circuits[17,18], endogenous circuits[19], cell–cell communication[20–22] and cellular computers[23], and can be implemented using RNA components[24–26], synthetic transcriptional regulation[27] or protein–protein interactions[28].

Using fundamental properties of the scaling laws of thermodynamic noise with temperature and molecular count, which hold in both biological and electronic systems, the advantages and disadvantages of analog computation versus digital have been analysed for neurobiological systems[3] and for systems in cell biology[5]. These results show that analog computation is more efficient than digital computation in part count, speed and energy consumption below a certain crossover computational precision. Although the exact crossover precision varies with the computation, both in electronics and in actual biological cells, the use of feedback loops, calibration loops, technological basis functions, redundancy, signal averaging and error-correcting topologies can push this crossover precision to higher values[3]. Alternatively,

for a given speed of operation, more energy must be expended in creating a higher molecular production rate, which leads to a higher molecular count and, thus, higher precision[3,5]. Trade-offs between error and resource use are therefore inherent in the design of synthetic circuits in living cells. To demonstrate the tunability of our analog circuits, we constructed an AraC PFS circuit with two P_{BAD} promoters on the shunt plasmid, leading to an increase in the log-linear gain of about twofold relative to the circuit's single-P_{BAD} counterpart (Supplementary Fig. 25). We have also analysed the sensitivities of our circuits, defined as the fractional change in the output divided by the fractional change in the input, and found that they compare favourably to circuits operating with positive feedback only or in open-loop configurations (Supplementary Fig. 27).

We propose that an efficient and accurate computational approach to synthetic biological networks will ultimately integrate both analog and digital processing (a simple example of switched analog computation is shown in Supplementary Fig. 24). This mixed-signal approach can utilize analog or collective analog computation[5] (the latter with many interacting moderate-precision analog circuits) for front-end processing in concert with decision-making digital circuits; or it may use graded feedback for simultaneous analog and digital computation, as in neuronal networks in the brain[29]. Thus, future efforts can seek to integrate synthetic analog and digital computation in living cells to achieve enhanced computational power, efficiency, reliability and memory. Such mixed-signal processing would benefit from the development of circuits to convert signals from analog to digital, and vice versa[5,30]. These complementary approaches promise to broaden the computational power of synthetic biology and the range of applications that can be addressed using techniques from this emerging engineering field.

METHODS SUMMARY

Strains and plasmids. All plasmids in this work were constructed using basic molecular cloning techniques (Supplementary Information). *Escherichia coli* 10β (araD139 Δ(ara-leu)7697 fhuA lacX74 galK (Φ80 Δ(lacZ)M15) mcrA galU recA1 endA1 nupG rpsL (StrR) Δ(mrr-hsdRMS-mcrBC)) or *E. coli* EPI300 (F- mcrA Δ(mrr-hsdRMS-mcrBC) Φ80dlacZΔM15 ΔlacX74 recA1 endA1 araD139 Δ(ara, leu)7697 galU galK λ- rpsL (StrR) nupG trfA tonA), where noted, were used as bacterial hosts for the circuits in Figs 1–3.

Circuit characterization. Overnight cultures of *E. coli* strains were grown from glycerol freezer stocks at 37 °C, in a VWR 1585 shaking incubator at 300 r.p.m., in 3 ml of Luria–Bertani–Miller medium (Fisher) with appropriate antibiotics: carbenicillin (50 μg m^{-1}), kanamycin (30 μg ml^{-1}), chloramphenicol (25 μg ml^{-1}). The inducers used were arabinose, isopropyl-β-D-1-thiogalactopyranoside and AHL 3OC6HSL (Sigma-Aldrich). Where appropriate, CopyControl[12] from Epicentre was added to overnight cultures at ×1 active concentration. Overnight cultures were diluted 1:100 into 3 ml fresh Luria–Bertani medium and antibiotics, and were incubated at 37 °C and 300 r.p.m. for 20 min. Cultures (200 μl) were then moved into 96-well plates, combined with inducers and incubated for 4 h 20 min in a VWR microplate shaker (37 °C, 700 r.p.m.), until they had an attenuance of $D_{600\,nm} \sim 0.6–0.8$.

Cells were then diluted fourfold into a new 96-well plate containing fresh ×1 PBS and immediately assayed using a BD LSRFortessa high-throughput sampler. Detailed characterization methods can be found in Supplementary Information. At least 50,000 events were recorded in all experiments, and these data were then gated by forward scatter and side scatter using CYFLOGIC v.1.2.1 software (CyFlo). The geometric means of the gated fluorescence distributions were calculated using MATLAB. Fluorescence values were based on geometric means of flow cytometry populations from three experiments, each of which corresponded to 50,000 events, and the error bars represent standard errors of the mean.

Full Methods and any associated references are available in the online version of the paper.

Received 10 October 2012; accepted 3 April 2013.
Published online 15 May 2013.

1. Chen, Y. Y., Galloway, K. E. & Smolke, C. D. Synthetic biology: advancing biological frontiers by building synthetic systems. *Genome Biol.* **13,** 240 (2012).
2. Cardinale, S. & Arkin, A. P. Contextualizing context for synthetic biology: identifying causes of failure of synthetic biological systems. *Biotechnol. J.* **7,** 856–866 (2012).
3. Sarpeshkar, R. Analog versus digital: extrapolating from electronics to neurobiology. *Neural Comput.* **10,** 1601–1638 (1998).
4. Ferrell, J. E. Signaling motifs and Weber's law. *Mol. Cell* **36,** 724–727 (2009).
5. Sarpeshkar, R. *Ultra Low Power Bioelectronics: Fundamentals, Biomedical Applications, and Bio-Inspired Systems* 651–694, 753–786 (Cambridge Univ. Press, 2010).
6. Sprinzak, D. *et al. Cis*-interactions between Notch and Delta generate mutually exclusive signalling states. *Nature* **465,** 86–90 (2010).
7. Canton, B., Labno, A. & Endy, D. Refinement and standardization of synthetic biological parts and devices. *Nature Biotechnol.* **26,** 787–793 (2008).
8. Giorgetti, L. *et al.* Noncooperative interactions between transcription factors and clustered DNA binding sites enable graded transcriptional responses to environmental inputs. *Mol. Cell* **37,** 418–428 (2010).
9. Clark, B. & Hausser, M. Neural coding: hybrid analog and digital signalling in axons. *Curr. Biol.* **16,** R585–R588 (2006).
10. Daniel, R., Woo, S. S., Turicchia, L. & Sarpeshkar, R. in *Biomedical Circuits and Systems Conference (BioCAS 2011)* 333–336 (IEEE, 2011).
11. Tavakoli, M. & Sarpeshkar, R. A sinh resistor and its application to tanh linearization. *IEEE J. Solid-State Circuits* **40,** 536–543 (2005).
12. Wild, J., Hradecna, Z. & Szybalski, W. Conditionally amplifiable BACs: switching from single-copy to high-copy vectors and genomic clones. *Genome Res.* **12,** 1434–1444 (2002).
13. Qian, L. & Winfree, E. Scaling up digital circuit computation with DNA strand displacement cascades. *Science* **332,** 1196–1201 (2011).
14. Stricker, J. *et al.* A fast, robust and tunable synthetic gene oscillator. *Nature* **456,** 516–519 (2008).
15. Elowitz, M. B. & Leibler, S. A synthetic oscillatory network of transcriptional regulators. *Nature* **403,** 335–338 (2000).
16. McMillen, D., Kopell, N., Hasty, J. & Collins, J. J. Synchronizing genetic relaxation oscillators by intercell signaling. *Proc. Natl Acad. Sci. USA* **99,** 679–684 (2002).
17. Madar, D., Dekel, E., Bren, A. & Alon, U. Negative auto-regulation increases the input dynamic-range of the arabinose system of *Escherichia coli*. *BMC Syst. Biol.* **5,** 111 (2011).
18. Nevozhay, D., Adams, R. M., Murphy, K. F., Josić, K. & Balázsi, G. Negative autoregulation linearizes the dose–response and suppresses the heterogeneity of gene expression. *Proc. Natl Acad. Sci. USA* **106,** 5123–5128 (2009).
19. Shen-Orr, S. S., Milo, R., Mangan, S. & Alon, U. Network motifs in the transcriptional regulation network of *Escherichia coli*. *Nature Genet.* **31,** 64–68 (2002).
20. You, L., Cox, R. S., Weiss, R. & Arnold, F. H. Programmed population control by cell–cell communication and regulated killing. *Nature* **428,** 868–871 (2004).
21. Tabor, J. J. *et al.* A synthetic genetic edge detection program. *Cell* **137,** 1272–1281 (2009).
22. Tamsir, A., Tabor, J. J. & Voigt, C. A. Robust multicellular computing using genetically encoded NOR gates and chemical 'wires'. *Nature* **469,** 212–215 (2011).
23. Auslander, S., Auslander, D., Muller, M., Wieland, M. & Fussenegger, M. Programmable single-cell mammalian biocomputers. *Nature* **487,** 123–127 (2012).
24. Isaacs, F. J. *et al.* Engineered riboregulators enable post-transcriptional control of gene expression. *Nature Biotechnol.* **22,** 841–847 (2004).
25. Win, M. N. & Smolke, C. D. Higher-order cellular information processing with synthetic RNA devices. *Science* **322,** 456–460 (2008).
26. Xie, Z., Wroblewska, L., Prochazka, L., Weiss, R. & Benenson, Y. Multi-input RNAi-based logic circuit for identification of specific cancer cells. *Science* **333,** 1307–1311 (2011).
27. Khalil, A. *et al.* A synthetic biology framework for programming eukaryotic transcription functions. *Cell* **150,** 647–658 (2012).
28. Dueber, J. E., Yeh, B. J., Chak, K. & Lim, W. A. Reprogramming control of an allosteric signaling switch through modular recombination. *Science* **301,** 1904–1908 (2003).
29. Hahnloser, R. H. R., Sarpeshkar, R., Mahowald, M. A., Douglas, R. J. & Seung, H. S. Digital selection and analogue amplification coexist in a cortex-inspired silicon circuit. *Nature* **405,** 947–951 (2000).
30. Lu, T. K., Khalil, A. S. & Collins, J. J. Next-generation synthetic gene networks. *Nature Biotechnol.* **27,** 1139–1150 (2009).

Supplementary Information is available in the online version of the paper.

Acknowledgements We would like to thank J. Nungesser for assistance with figures and members of the Lu and Sarpeshkar laboratories for discussions. This work was supported in part by a campus collaboration initiative from Lincoln Labs (R.D. and R.S.), the US National Science Foundation (R.D., J.R.R., R.S. and T.K.L.) under grant number 1124247, and the Office of Naval Research (J.R.R. and T.K.L.) under grant number N000141110725.

Author Contributions R.D., R.S. and T.K.L. designed the study. R.D. and J.R.R. performed experiments and collected data. R.D., J.R.R., R.S. and T.K.L. invented the analog circuit motifs. R.D., R.S. and T.K.L. developed the analog circuit motifs and associated models and simulations. All authors analysed the data, discussed results and wrote the manuscript.

Author Information Reprints and permissions information is available at www.nature.com/reprints. The authors declare competing financial interests: details are available in the online version of the paper. Readers are welcome to comment on the online version of the paper. Correspondence and requests for materials should be addressed to R.S. (rahuls@mit.edu) and T.K.L. (timlu@mit.edu).

METHODS

Strains and plasmids. All plasmids in this work were constructed using basic molecular cloning techniques (Supplementary Information). *Escherichia coli* 10β (araD139 Δ(ara-leu)7697 fhuA lacX74 galK (Φ80 Δ(lacZ)M15) mcrA galU recA1 endA1 nupG rpsL (StrR) Δ(mrr-hsdRMS-mcrBC)) or *E. coli* EPI300 (F- mcrA Δ(mrr-hsdRMS-mcrBC) Φ80dlacZΔM15 ΔlacX74 recA1 endA1 araD139 Δ(ara, leu)7697 galU galK λ- rpsL (StrR) nupG trfA tonA), where noted, were used as bacterial hosts for the circuits in Figs 1-3.

Circuit characterization. Overnight cultures of *E. coli* strains were grown from glycerol freezer stocks in a shaking incubator at 37 °C and 300 r.p.m. in 3 ml of Luria–Bertani–Miller medium (Fisher), with appropriate antibiotics: carbenicillin (50 μg ml^{-1}), kanamycin (30 μg ml^{-1}), chloramphenicol (25 μg ml^{-1}). The inducers used were arabinose, IPTG and AHL 3OC6HSL (Sigma-Aldrich). Where appropriate, CopyControl[12] from Epicentre was added to overnight cultures at ×1 active concentration. Overnight cultures were diluted 1:100 into 3 ml fresh Luria–Bertani medium and antibiotics, and were incubated at 37 °C and 300 r.p.m. for 20 min. Cultures (200 μl) were then moved into 96-well plates, combined with inducers and incubated for 4 h 20 min in a VWR incubating microplate shaker (37 °C, 700 r.p.m.) until they had an attenuance of $D_{600\,nm} \sim 0.6$–0.8.

Cells were then diluted fourfold into a new 96-well plate containing fresh ×1 PBS and immediately assayed using a BD LSRFortessa high-throughput sampler. Detailed characterization methods can be found in Supplementary Information. At least 50,000 events were recorded in all experiments, and these data were then gated by forward scatter and side scatter using CYFLOGIC v.1.2.1 software (CyFlo). The geometric means of the gated fluorescence distributions were calculated using MATLAB. Fluorescence values are based on geometric means of flow cytometry populations from three experiments and the error bars represent standard errors of the mean.

When they varied, inducers were titrated across rows through serial dilutions. When an inducer was kept constant, it was added to cultures before they were moved to 96-well plates.

Plate reader/FACS set-up. For each experiment, fluorescence readings were taken on a BioTek Synergy H1 Microplate Reader using BioTek GEN5 software to determine the minimum and maximum expression levels for cultures in each 96-well plate. GFP fluorescence was quantified by excitation at a wavelength of 484 nm and emission at a wavelength of 510 nm. mCherry fluorescence was quantified by excitation at 587 nm and emission at 610 nm. The gain of the plate reader was automatically sensed and adjusted by the machine.

Cultures containing the minimum and maximum fluorescence levels, as determined by the plate reader, were used to calibrate the fluorescein isothiocyanate and PE-TexasRed filter voltages on a BD LSRFortessa high-throughput sampler to measure GFP and mCherry expression levels, respectively. The FACS voltages were adjusted using BD FACSDIVA software so that the maximum and minimum expression levels could be measured with the same voltage settings. Thus, consistent voltages were used across each entire experiment. The same voltages were used for subsequent repetitions of the same experiment. GFP was excited with a 488-nm laser and mCherry was excited with a 561-nm laser. Voltage compensation for fluorescein isothiocyanate and PE-TexasRed was not necessary for any experiment. Supplementary Information, section 12, provides our FACS data.

Plasmid maps and construction. Supplementary Information, sections 13 and 14, provide details regarding plasmid construction and plasmid maps, respectively. The references in Supplementary Information, section 15, provide details regarding the origin of the plasmids.